Influence of HNT-ZnO Nanofillers on the Performance of Epoxy Resin Composites for Marine Applications

Raluca Şomoghi [1,2,*], Sonia Mihai [1], George-Mihail Teodorescu [2], Zina Vuluga [2], Augusta Raluca Gabor [2], Cristian-Andi Nicolae [2], Bogdan Trică [2], Daniel Mihai Stănescu Vătău [2], Florin Oancea [2] and Cătălin Marian Stănciulescu [3]

[1] Faculty of Petroleum Refining and Petrochemistry, Petroleum-Gas University of Ploiesti, 100680 Ploiesti, Romania; smihai@upg-ploiesti.ro
[2] National Institute for Research and Development in Chemistry and Petrochemistry—ICECHIM, Splaiul Independentei Street, No. 202, 6th District, 060021 Bucharest, Romania; georgemihail.teodorescu@yahoo.com (G.-M.T.); zvuluga@yahoo.com (Z.V.); ralucagabor@yahoo.com (A.R.G.); ca_nicolae@yahoo.com (C.-A.N.); trica.bogdan@gmail.com (B.T.); danystanescu@gmail.com (D.M.S.V.); florin@ping.ro (F.O.)
[3] Qwerty Development Macada-M Srl, Iancului Street, No. 29, 2nd District, 021716 Bucharest, Romania; catalin.stanciulescu@q-steel.ro
* Correspondence: r.somoghi@gmail.com

Abstract: Epoxy resin was conjugated with halloysite nanotubes (HNT) and different types of ZnO nanoparticles (commercial ZnO and modified ZnO-ODTES) to obtain HNT-ZnO/epoxy resin composites. These ZnO nanoparticles (ZnO NPs) were utilized with the intention to enhance the interfacial bonding between the epoxy resin and the reinforcing agent (HNT). The properties of resulted epoxy resin composites were characterized by various methods such as FTIR-ATR, TGA, DSC, TEM-EDX, and Nanoindentation analyses. The thermal properties of the epoxy resin composites were enhanced to a greater extent by the addition of HNT-ZnO nanofillers. DSC testing proved that the modification in the glass transition temperature can be due to the physical bonding between the epoxy resin and filler (HNT and/or ZnO). It was seen that the epoxy resin modified with HNT and ZnO-ODTES has the highest resistance to scratching by having a good elastic recovery as well as high values for surface hardness (~187.6 MPa) and reduced modulus (2980 MPa). These findings can pave the way for the developing of ZnO-based marine coatings with improved properties.

Keywords: epoxy resin; ZnO nanoparticles; thermal; nanoindentation

1. Introduction

Different types of coating have been continuously developed to achieve high-performance multifunctional coatings with scratch and abrasion resistance for the surface of various steel substrates for marine applications [1]. The most important characteristic of the coating is to be environmentally friendly and to achieve multi-functions, e.g., protection, high mechanical properties, fire resistance, and corrosion resistance. In order to obtain these improved surface properties, as well as protection against materials from hostile environments, optimized epoxy formulations are made incorporating nanoparticles like silica (SiO_2) and zinc oxide (ZnO) [2]. Epoxy systems tailored with metal-oxide nanoparticles can be used in automotive, aeronautic, construction and marine industries, because of their super adhesiveness to wide variety of surfaces, and the good thermo-mechanical properties [3]. Silica nanoparticles are frequently added into the polymer matrices to increase the heat resistance, radiation resistance, mechanical, and electrical properties of the final materials. The nano dimensions of the particles are very important for the properties of the acrylic-based coatings. The nano-silica particles are typically dispersed in the bulk polymer matrices using a suitable dispersing agent.

The epoxy resins have a high bonding strength and superior moisture resistance due to their ability to create chemical bonds or molecular adsorption as well as cross-links with curing agents. Due to their good physical, chemical and mechanical properties, epoxy resins are considered the best candidates as coating matrix [4]. Incorporating ZnO nanoparticles into epoxy resins can enhance the chemical resistance and the thermo-mechanical properties of composite coatings due to the formation of strong bonds that occur between oxide groups on the ZnO nanoparticles (ZnO NPs) surface and polar groups of epoxy resins [5]. Dispersion of nanosized particles into the epoxy matrix can prevent epoxy disaggregation and lead to the formation of homogeneous coatings [6,7]. Epoxy resins have disadvantages such as very strict conditions of utilizations, brittleness, low hardness, and low impact resistance, which limit their wide application.

Several research papers have reported the successful incorporation of ZnO NPs into epoxy resin in order to obtain high-performance composites. Sunny et al. showed that the addition of ZnO NPs to epoxy resins can improve the thermal and mechanical properties of the final composites [8]. Suntako revealed that the introduction of ZnO NPs enriched the properties of natural rubber such as tensile strength, hardness, and elongation at break [9]. Ding et al. [10] demonstrated that the incorporation of ZnO particles having submicron sizes (~100–200 nm) enhanced the tensile and flexural strength of epoxy resin by 41 and 51%, respectively. Thipperudrappa et al. [11] showed that the ZnO NPs improved the mechanical properties of reinforced epoxy composites (2 wt% of ZnO). Liu et al. [12] obtained epoxy nano-composites with good thermal and mechanical properties, using hybrids containing multi-walled carbon nanotube and ZnO NPs. Samad et al. [13] reported that the addition of ZnO nanoparticles to the epoxy matrix containing epoxy/polyaniline improved its mechanical and thermal properties. Effect of cadmium oxide (CdO) doped zinc oxide nanoparticles (ZnO NPs) on structural, thermal, mechanical and electrical properties of the epoxy composite was investigated and reported by Srikanth et al. [14]. Different concentrations of CdO-ZnO nanopowder into the epoxy matrix were used. They found that the epoxy composites prepared with 1 wt% concentration of CdO-ZnO in epoxy improved the tensile, flexural and compression properties. Hardoň et al. [15] demonstrated the influence of ZnO NPs (1 wt% and 5 wt% concentrations) on the dielectric properties of the epoxy resin. The experimental results showed that the epoxy resin containing ZnO filler with 1 wt% concentration present a lower relative permittivity for frequencies higher than 5 Hz because of the presence of very immobile epoxy chains in the interfacial regions around nanoparticles. Al-Lhaibi et al. [16] revealed that the surface roughness of sawdust/epoxy composites can be increased by increasing the ZnO NP content in the polymer matrix. Lorero et al. [17] developed a method to fabricate epoxy composites with recycled ZnO particles from spent alkaline batteries. The composite reinforced with 30 wt% recycled ZnO particles presented good thermomechanical properties (glass transition temperature (1.4%), stiffness (19.2%) and hardness (82.3%)). Guo et al. [18] demonstrated that the epoxy resins containing tetrapod-shaped ZnO whiskers present a superior thermal transport property in comparison to ZnO micron particles. Hawkins et al. [19] reported the preparation of epoxy resin composites containing ZnO and multi-walled carbon nanotubes, presenting high conductivity and improved elastic modulus. Halder et al. [20] obtained the epoxy composites with improved thermal and mechanical properties, using a lower concentration (2 wt%) of poly vinyl alcohol (PVA)-assisted ZnO NPs. Sari et al. [21] reported the effects of starch-modified ZnO NPs on the viscoelastic and mechanical properties of epoxy-based nanocomposite films. The obtained results revealed that the epoxy network becomes stiffer by introducing the modified ZnO particles. Also, Shi et al. [22] investigated the effect of different nanofillers (SiO_2, Zn, Fe_2O_3 and halloysite clay) on the corrosion resistance of epoxy coatings. The results obtained indicated that the corrosion resistance of the epoxy coatings was improved due to the increase in adhesion of the epoxy coating to the metal substrate. Tonelli et al. [23] reported that the addition of a small amount of halloysite clay nanotubes (HNTs) in epoxy coatings enhanced the antifouling properties of material. Kaybal et al. [24] showed that the halloysite nanotube (HNT) can improve the bearing

strength basalt-epoxy composite. Although the nanofillers show increased resistance compared to the pure properties of the polymer, their use in large quantities can lead to the formation of agglomerates and to a decrease in the adhesion of the epoxy coating to the metal substrate [25]. The aim of this study is to report the effect of halloysite nanotubes (HNT) and ZnO nanoparticles (commercial ZnO and modified ZnO-ODTES), as nanofillers, on the physico-chemical properties of epoxy resin. The morphology of these materials was analyzed using a Transmission Electron Microscope (TEM) analysis. Chemical composition of the samples was assessed using Fourier-Transform Infrared (FTIR) spectroscopy and Energy-Dispersive X-ray Spectroscopy (EDX). The glass transition temperature was determined using a differential scanning calorimeter (DSC). Thermogravimetric analysis (TGA) was used to investigate the performance of the synthesized epoxy resin composites. Nanoindentation and nano-scratching techniques were utilized to examine the nanomechanical surface properties of epoxy resin systems. The use of HNT as a reinforcing agent allows obtaining high-performance materials at a lower price compared to carbon nanotubes. To our best knowledge, the effect of HNT-ZnO nanofillers on the nanomechanical properties of the epoxy resin composites has not been studied to date. The modified ZnO/epoxy resin composites with balanced thermal and mechanical properties achieved in this study are designed for marine applications, and especially for shipping devices.

2. Experimental

2.1. Materials

Commercial zinc oxide nanopowder (ZnO, ZnO NPs < 100 nm, Sigma-Aldrich, Philadelphia, PA, USA), octadecyltriethoxysilane (ODTES, 98%, Alfa Aesar, Karlsruhe, Germany), xylene (Xy, S.C. Chimreactiv S.R.L., Bucharest, Romania), Tetraethyl orthosilicate (TEOS, 98%, Sigma-Aldrich, Philadelphia, PA, USA), methyl isobutyl ketone (MIBK, Sigma-Aldrich, Millipore, ON, Canada), ammonium hydroxide (NH_4OH, 32%, Scharlau, Sentmenat, Spain), epoxy resin (Resin 530 (component A (bisphenol A/F–epoxy resin) + hardener B (modified polyamine)), LEUNA-Harze GmbH, Leuna, Germany), and natural aluminosilicate clay with a hollow tubular morphology (HNT 100%, NaturalNano Corp., Rochester, NY, USA) were used as purchased.

The metal substrates are made of SRJ235 carbon steel, cut in the form of triangles with a base of 13 cm and sides of 21 cm. The metal substrates were placed in seawater taken from the Black Sea, with a salinity of 1%, and immersed for 6 months before scratching tests.
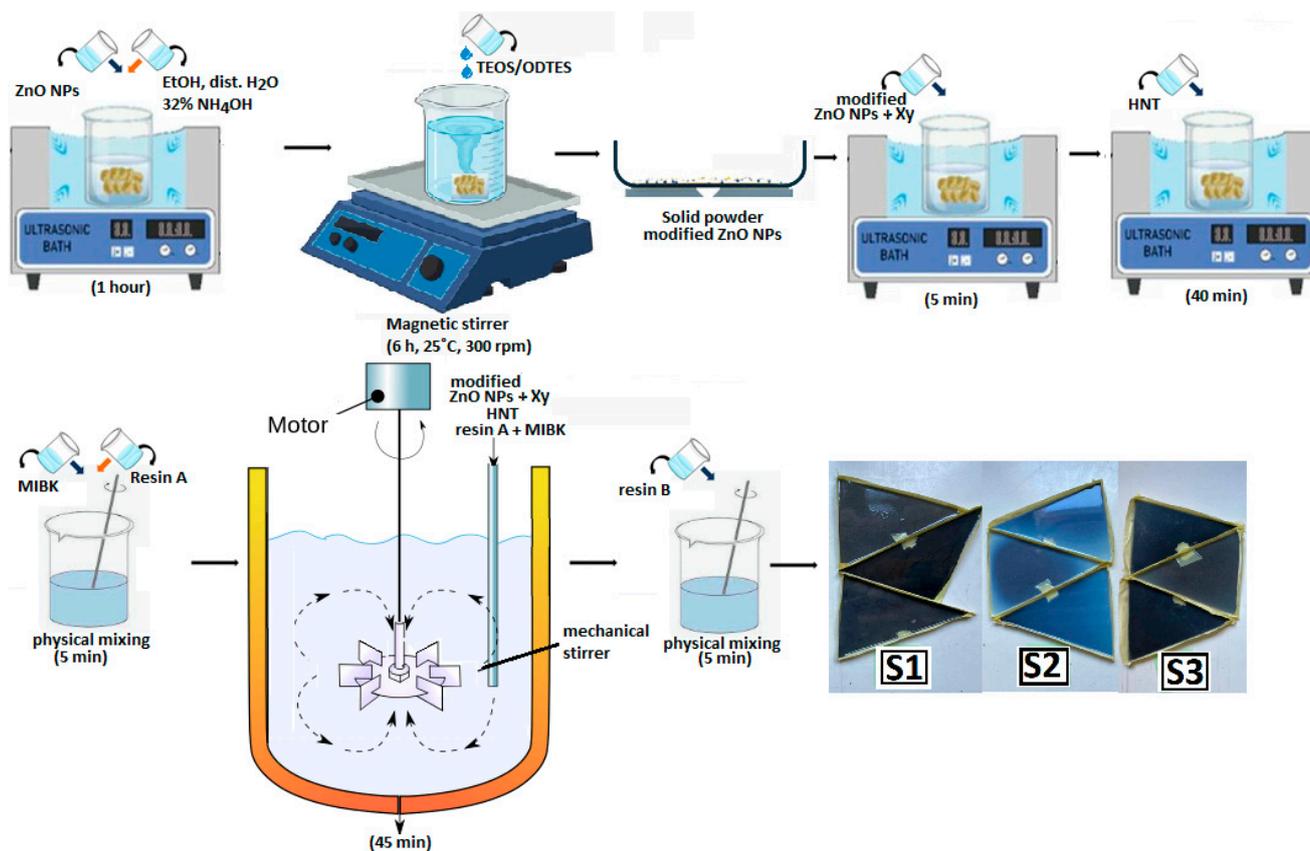
2.2. Preparation

ZnO nanoparticles (ZnO NPs) modified with ODTES were prepared using the method described in our previous studies [26,27]. A small amount of commercial ZnO nanopowder (1 g) was dispersed in a mixture containing ethanol (400 mL), demineralized water (100 mL) and ammonium hydroxide solution (32%, 10 mL) and sonicated for one hour in an ultrasonic bath. Tetraethyl orthosilicate (TEOS, 4.5 mL) and octadecyltriethoxysilane (ODTES, 9.5 mL) were added dropwise over the formed solution (molar ratio of TEOS/ODTES = 1/1). The resulting solution was magnetically stirred for 6 h, at room temperature (25 ± 2 °C).

Processing steps for epoxy resin are the following. The modified ZnO with xylene (Xy) was sonicated for 5 min in an ultrasonic bath. Aluminosilicate clay with a hollow tubular morphology (HNT) was then added and left to be ultrasonicated for 40 min. Methyl isobutyl ketone (MIBK) was poured over component A from the epoxy resin and manually mixed with it for 5 min. All these components were mixed for 45 min with a mechanical stirrer (800 rpm). The mechanical agitator head's shape was specifically designed to prevent bubbles from forming in the material. The last stage involved physically combining resin A with all integrated components and hardener B for five minutes. Three types of modified epoxy resin composites were finally obtained: HNT/epoxy resin (S1), HNT/ZnO/epoxy resin (S2) and HNT/ZnO-ODTES/epoxy resin (S3) (see Table 1). The final materials were coated onto the metal substrates and left for 48 h at room temperature for complete curing.

Table 1. Chemical composition of synthesized samples S1–S3.

Sample	Resin A (g)	Hardener B (g)	MIBK (g)	Xy (g)	HNT (g)	ZnO-ODTES (g)	Commercial ZnO (g)
S1						-	-
S2	66.6	33.3	8	8	5	-	1
S3						1	-

The schematic illustration of synthesis procedure to obtain modified ZnO/epoxy resin composites is shown in Figure 1.

Figure 1. Schematic illustration of synthesis procedure to obtain modified ZnO/epoxy resin composites.

2.3. Characterization

FTIR spectra of materials were recorded on a Spectrometer Tensor 37 (Bruker Instrument, Woodstock, NY, USA), in ATR (Attenuated Total Reflectance) mode with a Golden Gate diamond unite (spectral range of 4000–400 cm^{-1}, resolution of 4 cm^{-1}, 30 scans per spectrum).

Thermal analysis of the synthesized materials (dried under vacuum at 50 °C for 24 h) was undertaken in a Thermogravimetric Analyzer TGA Q5000IR (TA Instruments, New Castle, DE, USA) in a N_2 atmosphere (heating rate of 10 °C/min, from 30 °C at 750 °C). Obtained materials (3–5 mg) were analyzed using alumina crucibles.

A Differential Scanning Calorimeter (DSC Q2000, TA Instruments Inc., New Castle, DE, USA) was used to determine the temperature and heat flow associated with material transitions as a function of time and temperature. The experiments were performed with modulated temperature (MDSC). MDSC analysis was conducted under helium flow (25 mL/min), with a rate of 10 °C/min, and a period of 30 s as follows: equilibrating at −50 °C; isothermal for 2 min; and heating from −50 °C to 200 °C. In the Modulated Differential Scanning Calorimetry (MDSC), the heat flow (Total Heat Flow) was equivalent to standard DSC; the reversing heat flow provided information on reversible phase changes

(glass transition and melting), while the non-reversing heat flow showed just the kinetic (non-reversible) processes, such as enthalpic recovery at T_g, solvents evaporation, and chemical reactions.

The materials were analyzed through Transmission Electron Microscopy (TEM, model TECNAI F20 G^2 TWIN Cryo–TEM, FEI Company, Eindhoven, The Netherlands) at 200 kV accelerating voltage. The associated EDX spectra were obtained using the X-MaxN 80T detector (Oxford Instruments, Oxford, UK), installed on the device.

The Hysitron TriboIndenter Premier (TI) (Premier Hysitron, Minneapolis, MN, USA) device was employed to carry out nanomechanical testing. The hardness, reduced modulus, load–displacement curves along with the coefficient of friction and surface roughness were measured using nanoindentation and nano-scratching methods. The measurements were performed, adhering to the Oliver–Pharr method. A three-side Berkovich tip was used, with total angles of 142.35 degrees and a radius of curvature of 150 nm, while a 700 μN normal load force for nanoindentation and a 1000 μN load force for nano-scratching were applied to the surface of the samples according to their respective functions. The surface topography data was acquired by the TI Premier's Scanning Probe Microscopy mode (SPM), exhibiting representative 25 × 25 μm in situ images of the samples after the scratching procedure.

Scratch tests were performed using an Elcometer 3086 Motorized Pencil Hardness Tester (Elcometer, Manchester, UK) at 23 °C and 50% relative humidity with the applied force of 8 N. The method was used in accordance with the standard Standard Test Method for Film Hardness by Pencil Test ASTM D 3363 [28].

3. Results and Discussion

3.1. FTIR-ATR Spectroscopy

The chemical bonds present in the samples were analyzed using FTIR-ATR spectroscopy, and a plot of absorbance versus wave number is shown in Figures 2 and 3.
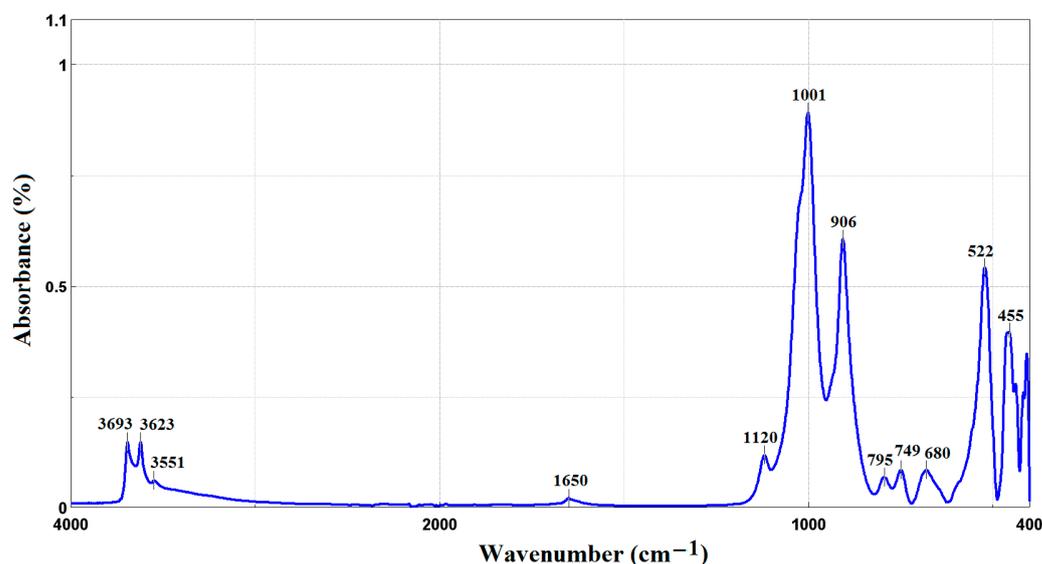

Figure 2. FTIR-ATR spectrum of HNT.

The FTIR spectrum of HNT is presented in Figure 2. Two sharp bands are observed at ~3697 and ~3625 cm^{-1}, which can be assigned to the stretching vibration of the inner-surface O–H bonds and due to the inner O–H groups near the aluminum atoms, respectively [29]. The absorption peaks at 1650, 906 and 1001 cm^{-1} can be seen and are assigned to O–H deformation of water, O–H bending of inner hydroxyl groups and Si–O stretching vibrations, respectively [30].

FTIR spectra of synthesized epoxy resin composites are showed in Figure 3. The band that appears at ~3340 cm^{-1} can be assigned to stretching vibrations of O–H groups [31]. The peaks located at 2922 and 2852 cm^{-1} are associated with –CH$_2$ and –CH$_3$ of aromatic

and aliphatic chains (stretching vibrations) [32,33]. Peaks in the interval of 1580–1610 cm^{-1} correspond to primary amine (N–H) [34]. The peak centered at 1508 cm^{-1} was attributed to N–O stretching vibration, indicating the presence of nitro compounds. According to literature, the C–C and C–O bonds (stretching vibrations) are observed at 1454 cm^{-1} and 1240 cm^{-1}, respectively [1,34]. The peaks in the range from 1000 to 1100 cm^{-1} correspond to C–N groups and indicate curing of the epoxy and the hardener. The peaks identified at 1181 cm^{-1} and ~1032 cm^{-1} are assigned to the asymmetrical aliphatic C–O stretching vibrations [33,35]. The peak at 826 cm^{-1} is associated with the 1,4-substitution of the aromatic ring of the epoxy resin (R). The increase in the intensity of this peak may indicate a significant presence of the epoxide ring [36].
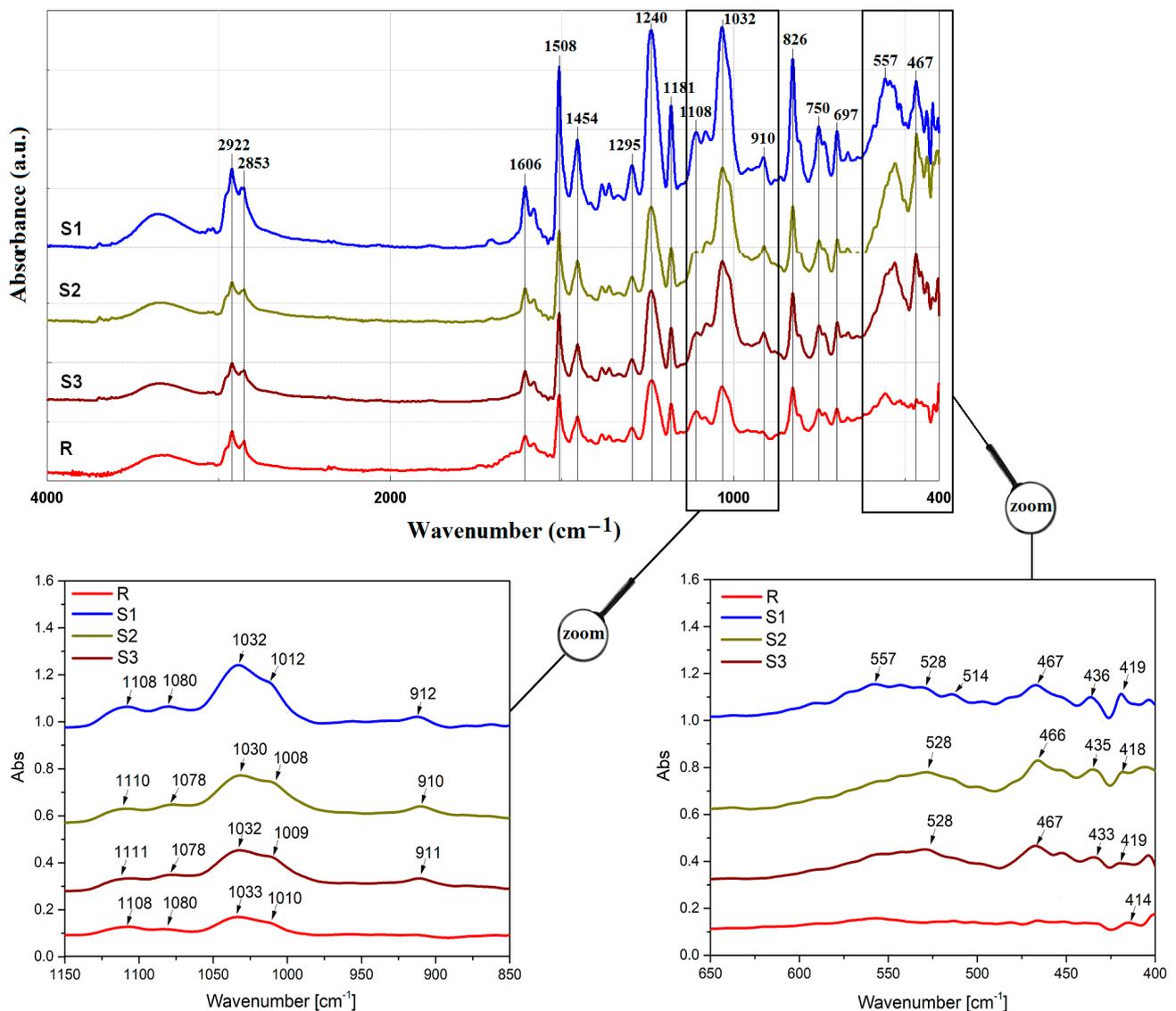

Figure 3. FTIR-ATR spectra of samples S1–S3 and of epoxy resin (R).

The peak identified at ~910 cm^{-1} is observed in the FTIR spectra of samples S1–S3 and is associated with Si–O bending vibrations [27]. The peaks located at ~1010/1032 cm^{-1} and ~1110 cm^{-1} are attributed to the OH deformation of inner hydroxyl groups from Al–OH and to the Si–O bonds (in-plane and perpendicular stretching vibrations), respectively [37]. The peaks located at 467 cm^{-1}, 528 cm^{-1} and ~436 cm^{-1} are attributed to Si–O–Si bond bending vibrations and to the Si–O–Si deformation band [38,39].

Bands identified at ~1100 cm^{-1} and ~1080 cm^{-1} (aromatic stretching) show changes in intensity. The intensity increase of peak at ~1080 cm^{-1} can be attributed to the connection of the hydroxyl in the molecular backbone of the modified epoxy resin composites (samples S2 and S3) with the secondary carbon atom [40]. In the FTIR spectra of all samples S1–S3, an increase in peak intensity was noticed for Si–O stretching vibrations, which may be due to the effect of HNT–epoxy interactions [41].

Taking into account the molecular structures of the involved partners (epoxy resin, HNT and ZnO NPs fillers) and FTIR results, some combinations of interactions (e.g., electrostatic forces, van der Waal forces, covalent bonding, hydrogen bonds, and hydrophobic interactions) that have different energies may occur during the processing steps.

3.2. TGA and DSC Analysis

Figure 4 reveals the TGA analysis of the synthesized epoxy resin composites (samples S1–S3). The decomposition temperature (T_{max}) and the weight loss (Wt. loss %) of these samples are presented in Table 2.
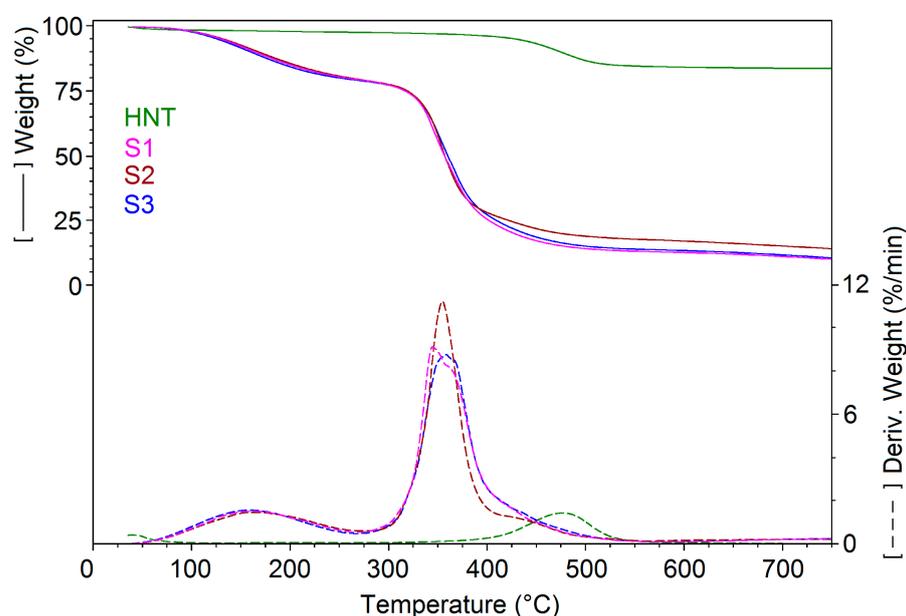

Figure 4. Thermogravimetric analysis curves of samples: HNT, S1, S2, S3 and S4.

Table 2. The maximum decomposition temperature (T_{max}) and weight loss (Wt. loss %) of the prepared composites and of HNT (temperature range of 30–750 °C).

Sample	30–265 °C		265–575 °C		575–750 °C	Residue at 750 °C
	Wt. loss %	T_{max} [1] °C	Wt. loss %	T_{max} °C	Wt. loss %	N$_2$ %
HNT	2.04	201.6	13.22	476.7	0.64	84.10
S1	20.20	162.0	66.85	344.6	2.77	10.19
S2	20.44	165.1	61.78	354.6	3.49	14.28
S3	20.46	158.1	65.76	358.4	3.06	10.72

[1] T_{max} (°C) = T (dα/dt)$_{max}$.

From the TGA curves, it can be observed that the decomposition of the synthesized epoxy resin composites occurred around 150 °C. A weight loss of 15%–20% up to the temperature of 160 °C (where a maximum occurs) may be due to the removal by volatilization of some compounds (e.g., xylene and methyl isobutyl ketone, 5% loss) present in the synthesized resins (see Table 2).

It can be seen from Figure 4 and Table 2 that the major mass loss of HNT occurs rapidly at about 480 °C, assigned to the dehydroxylation of structural aluminol groups present in HNT [42].

Muhammad et al. [43] demonstrated that the ZnO NPs improved the stability of the epoxy coatings after exposure under environmental conditions.

The enthalpy phenomena observed in DSC curves are associated with the mass loss highlighted in TGA analysis, for the 100–250 °C range.

As can be seen from Figure 5, the events that take place between 70–200 °C range are irreversible kinetic processes due to the evaporation of volatile materials (solvents), which are represented by the approximately 12%–15% mass loss recorded in TGA analysis. Due to the removal of volatile materials, the resins stiffened and upon the second heating, the glass transition (T_g) moved to values between 85–90 °C, after which there was no further thermal event until 200 °C.
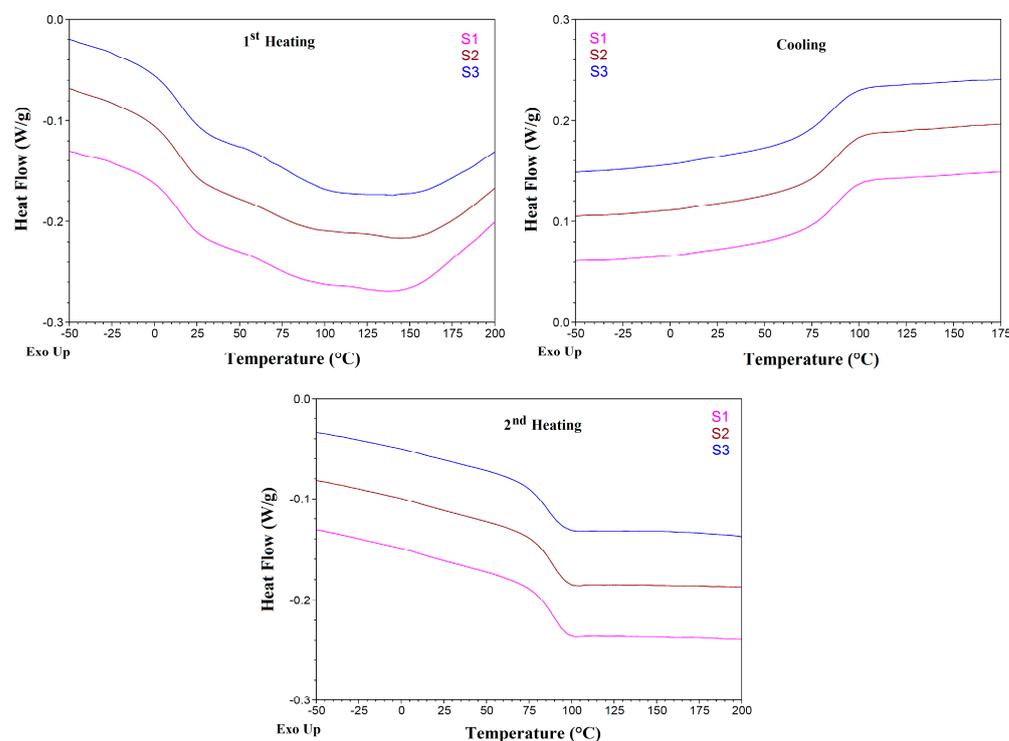

Figure 5. DSC curves of samples (top—first heating; down—second heating) S1–S3.

After 200 °C, the volatile compounds were removed and the material hardened. As can be seen in the cooling and the 2nd heating curves (Figure 5), T_g moved to higher temperatures and increased above 70 °C. After applying the resin, the final materials were hardened, having T_g values comparable to T_g values for other polymers such as polyethylene terephthalate (PET, 67–81 °C) and polyvinyl chloride (PVC, 82 °C) (see Table 3). The polymer chains slid can past each other at lower temperatures, resulting in a decrease in T_g [44].

These results are in agreement with those reported in the literature [45,46], where it was shown that the addition of ZnO nanoparticles decreased the thermal properties of the materials because ZnO tends to form free oxygen and oxygen vacancies. In addition, it can be seen that the percentage of residue increased with the addition of inorganic molecules on the ZnO nanoparticles, as they do not decompose in the evaluated temperature range [46]. Also, it was shown that the T_g of polymer matrix and crosslinking could decrease because of the aggregate formations or the imperfect solutions, even at contents below 2 wt% ZnO [47].

Table 3. Values of T_g temperatures determined by DSC for samples S1–S3.

	Glass Transition										
	1st Heating				Cooling				2nd Heating		
Sample	Onset (°C)	T_g (I) (°C)	End (°C)	ΔCp J/(g °C)	Onset (°C)	T_g (I) (°C)	End (°C)	ΔCp J/(g °C)	Onset (°C)	T_g (I) (°C)	End (°C)	ΔCp J/(g °C)
S1	1.5	14.4	25.7	0.33	99.7	89.7	72.0	0.33	77.1	88.9	96.6	0.30
S2	0.6	14.1	26.0	0.35	99.5	87.1	70.8	0.34	76.7	88.1	96.9	0.30
S3	2.3	15.0	27.8	0.35	97.7	85.8	68.2	0.32	73.4	85.6	95.2	0.30

Adroja et al. [48] demonstrated that the curing kinetics were influenced by steric restrictions on the epoxy–amine addition reaction, physical interactions between the various functional groups of the constituent components, and the extent of curing.
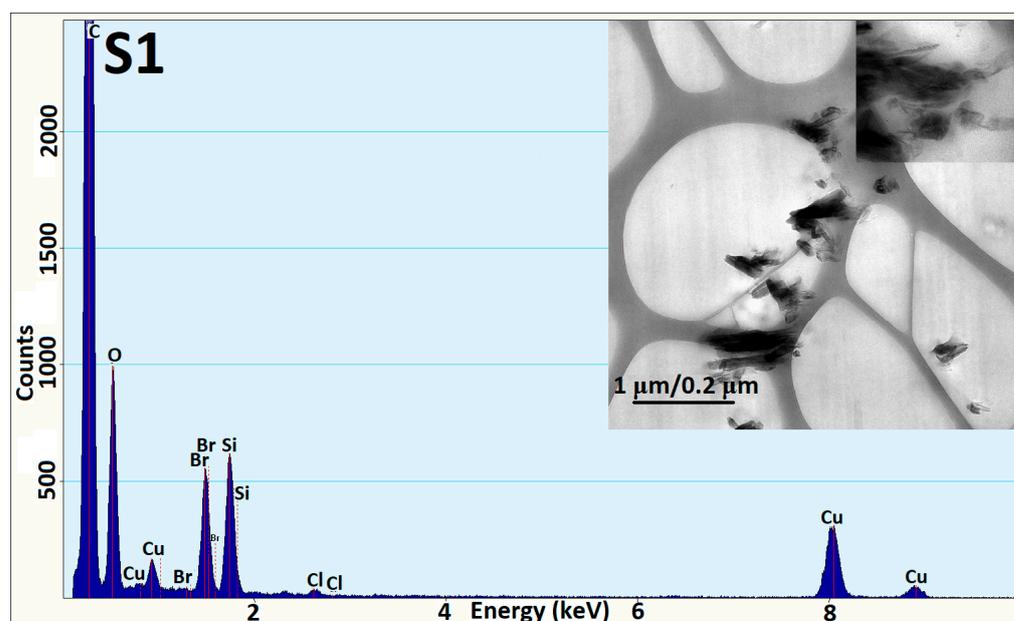
3.3. TEM Analysis

The morphology and elemental analysis of the samples were assessed by Transmission Electron Microscopy (TEM) equipped with energy-dispersive X-ray (EDX). The TEM images and EDX analysis are illustrated in Figure 6.

Through TEM imaging, the presence of HNT nanotubes was observed in all three samples. In samples S2 and S3, the presence of ZnO NPs was also determined. Sample S1 is the one that does not present any kind of ZnO NPs. Moreover, the images reveal that the HNT and used ZnO NPs do not tend to form any agglomerates in the structure of samples. Aside from some small cavities on the synthesized epoxy resin composite surface, a strong coherent bonding between the interfacial layers of epoxy resin and the fillers (HNT or ZnO NPs) was noticed.

Consequently, distribution of the fillers (HNT or ZnO NPs) in the compositions led to the formation of samples without high agglomerations or sedimentation.

From EDX analysis, the existence of Zn signals could be detected in samples S2 and S3, originating from ZnO NPs utilized in synthesis. Due to the present of Cu line scan, it can be concluded that the carbon foil on the TEM copper grid may be responsible for the signals.
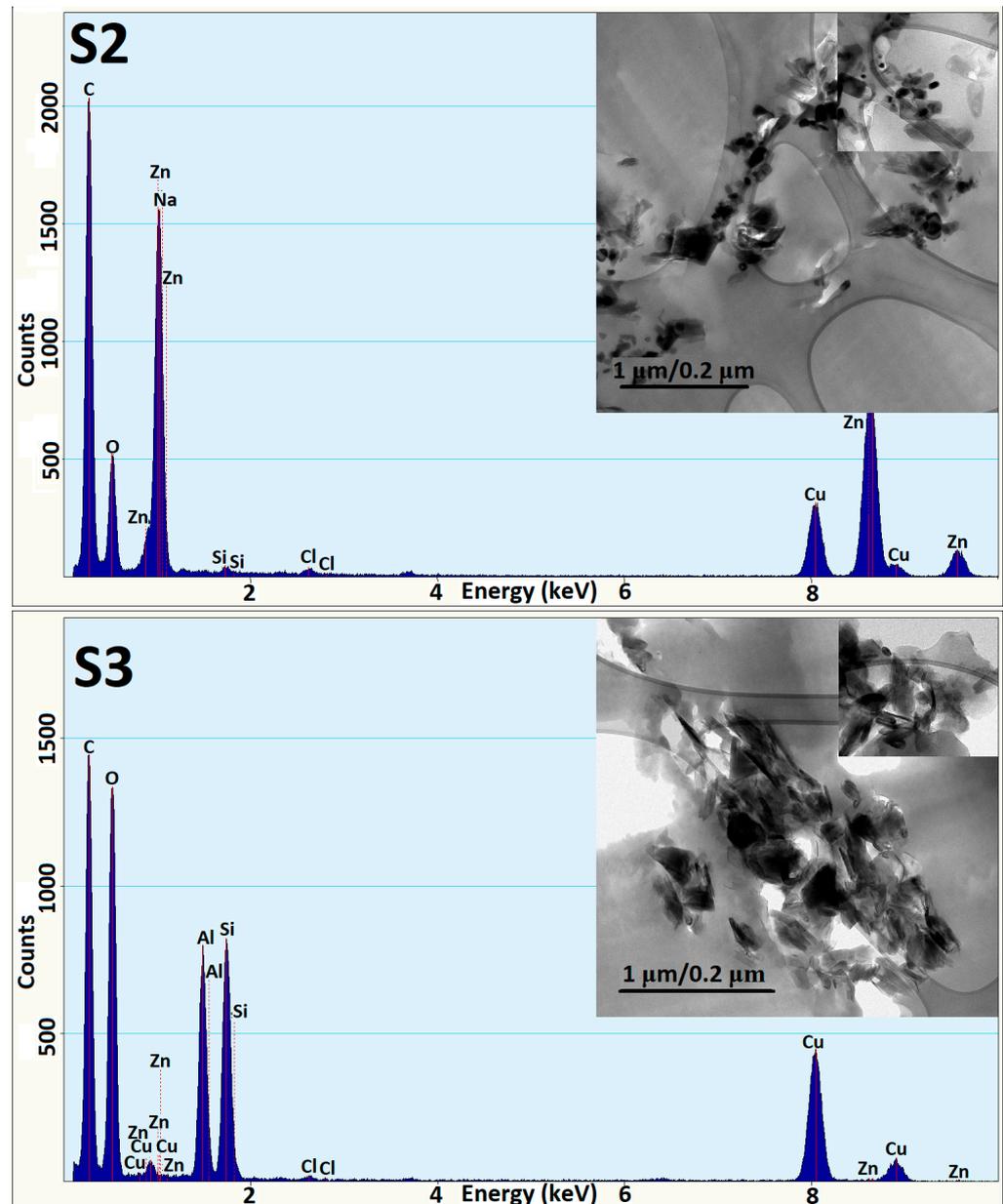

Figure 6. *Cont.*

Figure 6. TEM images and EDX analysis of samples S1–S3.

3.4. Nanoindentation Analysis Method

Nanomechanical characterization was performed on specimens of 10 mm × 10 mm × 4 mm (length × width × thickness), obtained by casting process into a silicon mold at room temperature with the curing time of 24 h, to determine the surface hardness and modulus by employing a nanoindentation technique.

From Figure 7a,b, it can be seen that sample S3 conjugated with HNT and ZnO-ODTES had the highest values for hardness (~187.6 MPa) and reduced modulus (2980 MPa), although the difference between the values is quite small, compared to samples S1 and S2. Also, it can be observed that sample S3 has the lowest degree of elastic recovery (see Figure 7b). Lizundia et al. [49] showed that the epoxy nanocomposites functionalized with SiO_2 nanoparticles present the storage modulus of ~2725 MPa. In comparison with this nano-filler (SiO_2 nanoparticles) that was employed for improvements of mechanical properties of epoxy nanocomposites, the present study indicates that the incorporation of HNT-ZnO NPs into epoxy composites enhances the performance of epoxy resin material.
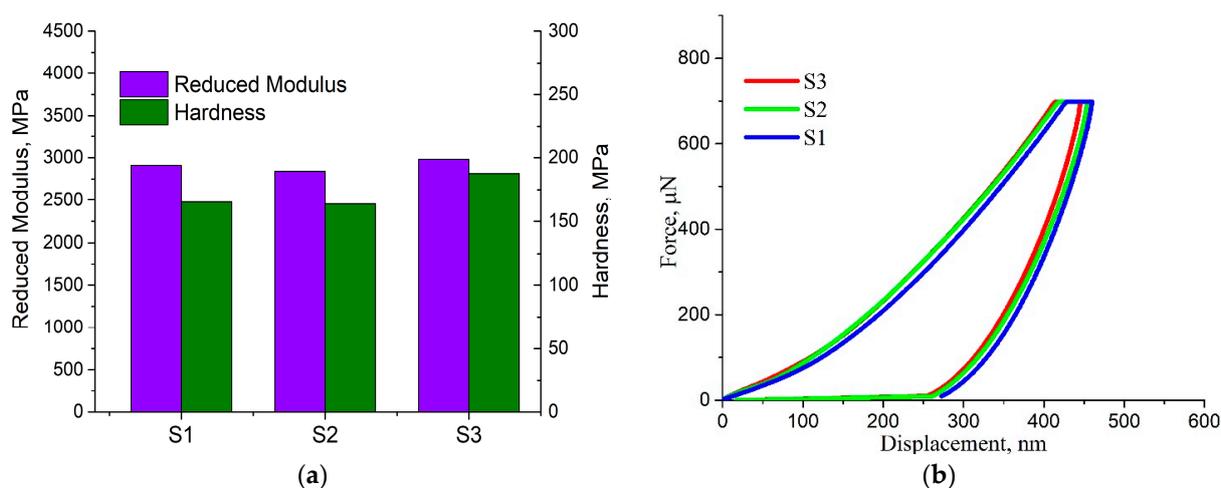
Figure 7. (**a**) Indentation reduced modulus and hardness; (**b**) force vs. displacement curves of samples S1–S3.

It is well known that the reduced modulus and hardness of polymer composites are highly dependent on the interfacial adhesion between the filler and the matrix. Panahandeh et al. [50] demonstrated that the agglomeration of ZnO on the surface can increase the chances of their indentations. Accumulation of some agglomerates on the surface and the partial cross-linking of the resins can decrease the mechanical properties of the composite. Li et al. [51] reported similar results where a decrease in properties was observed after exceeding 2% ZnO loading rate. Our study will continue by optimizing the mixing and crosslinking parameters as well as the working conditions.

In the present study, nano-scratching was done to obtain more data regarding the coefficient of friction, roughness and the surface topography under mechanical stress for the samples.

Scanning probe microscopy (SPM), as seen in Figure 8a–c, shows that the synthesized epoxy composites (samples S1–S3) present some differences (aggregates with different shapes). The Rms roughness (root-mean-square roughness) and the coefficient of friction of the synthesized epoxy resin composites are indicated in Table 4. Sample S3 shows the most formations and agglomerates, which can be seen both on the surface and inside the semi-transparent sample. The differences in surface roughness for samples S1–S3 were of approximately 25 nm, 23 nm and 13 nm, respectively. These values as well as those obtained from nanoindentation indicate that, out of the three epoxy composites, sample S3 has the highest resistance to scratching by having a good elastic recovery as well as high values for surface hardness and reduced modulus, as seen in Figure 7a,b. Sample S1 has very low roughness values before and after scratching as a result of the difference between the highest and lowest point on the image. Compared to the other samples, it seems that sample S1 has a smooth surface and the presence of the scratch does not lead to an increase in surface roughness. The reasons for the lower properties of sample S1 are maybe due to the weak in particle-to-particle interaction, and poor aggregation of HNT in the epoxy matrix.

Table 4. Rms roughness (root-mean-square roughness) and coefficient of friction values of samples S1–S3.

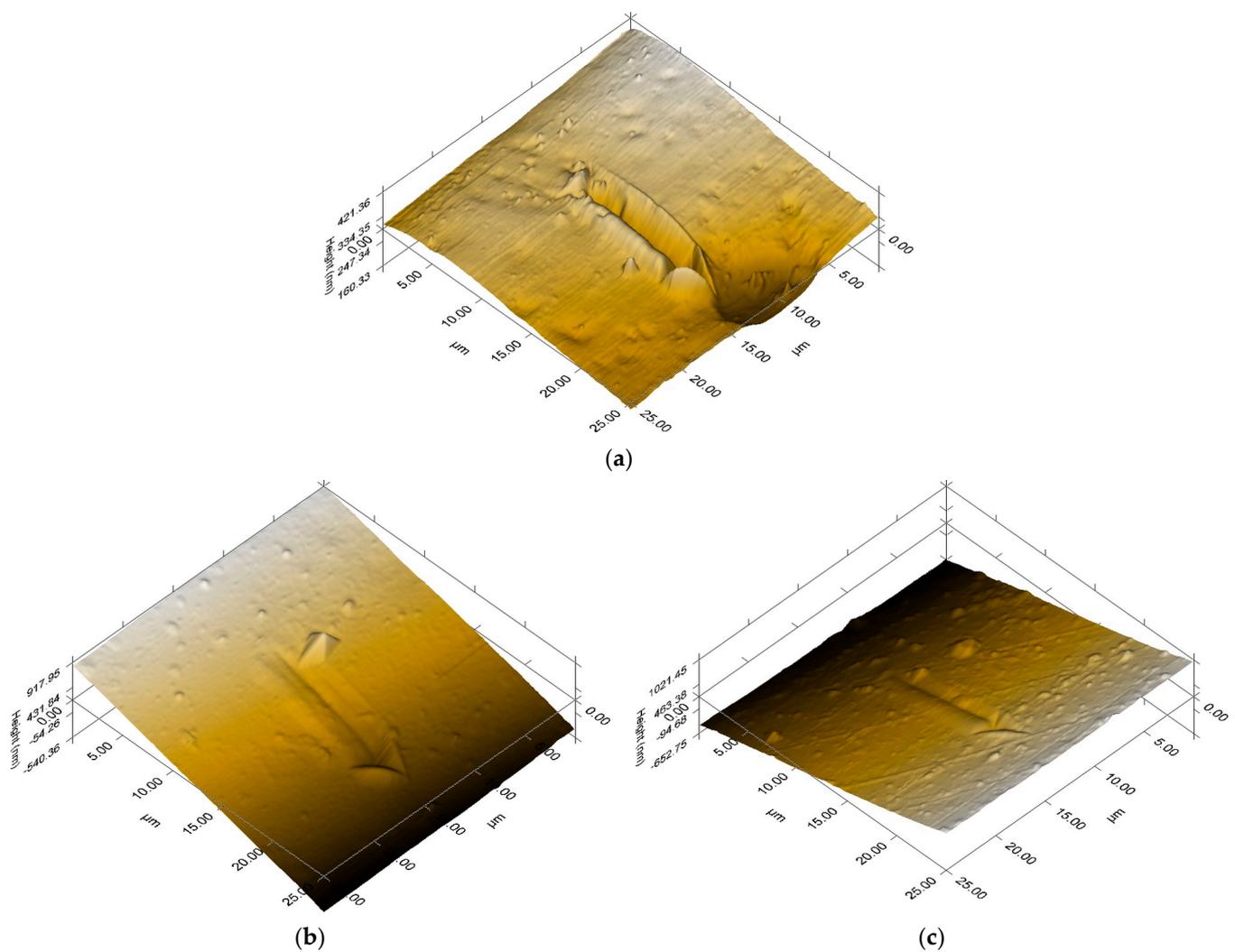| Sample	Roughness (Rms, nm)		Coefficient of Friction (µ)
	Before Scratch	**After Scratch**	
S1	65.007	40.170	0.40 ± 0.04
S2	423.812	401.013	0.40 ± 0.04
S3	418.214	430.878	0.40 ± 0.06

Figure 8. Three-dimensional plot of SPM image after scratching for samples: (**a**) S1; (**b**) S2; (**c**) S3.

A lower coefficient means that the materials will have higher wear resistance. Out of the three modified epoxy resin composites, sample S3 has optimal properties for the final applications of the composite, especially in the naval field where the surface is constantly subjected to the forces of friction and impact with seawater.
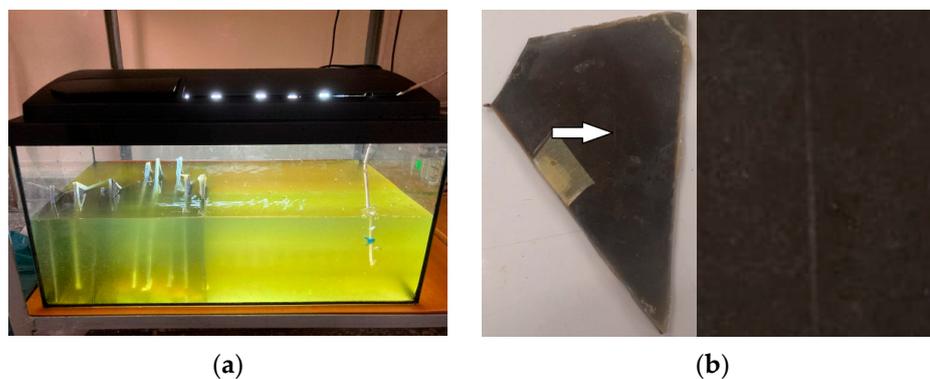
Karasinski et al. [52] demonstrated that the utilization of ZnO NPs actions as a barrier against an external indentation force, leading to superior properties due to excellent charge transferability between polymer matrix and filler.

Similar results were achieved by Cristea et al. [53] where the indentation modulus and hardness were increased due to the increased stiffness of the samples. Also, it was concluded that the distribution of the filler in the polymer matrix can notably affect the indentation results. The polymer material could exhibit an increase in modulus if exposed to accelerate weathering [54]. The scratch tests were performed using a wide range of lead with different hardness (2H > H > B). Metal surfaces coated with modified epoxy resin were kept in seawater for 6 months before the scratching tests (see Figure 9). The results presented in Table 5 are focused on the range of lead hardness where a change in scratching behavior occurs.

The obtained results indicated that samples S2 and S3 have a higher resistance to scratching compared to sample S1 as a higher hardness lead was required in order to leave a visible scratch pattern on the surface of the samples.

Table 5. Scratch tests results for samples S1–S3.

Sample	2H	H	B
S1	Visible scratch	Visible scratch	No visible scratch
S2	Visible scratch	No visible scratch	No visible scratch
S3	Visible scratch	No visible scratch	No visible scratch

(**a**) (**b**)

Figure 9. (**a**) Metal surfaces coated with samples and kept in seawater; (**b**) sample S3 after scratching test (the scratch is pointed by the white arrow).

Parimalam et al. showed that the epoxy/SiO_2/ZnO coating presented a lower adhesive property than the epoxy/SiO_2/TiO_2/ZnO/rubber latex nanocoating [55].

Analyzing the results presented in this study, it can be concluded that the addition of a small amount of HNT-ZnO nanofillers in epoxy coatings can lead to an improvement in the physico-chemical properties of the material.

4. Conclusions

The effect of HNT-ZnO nanofillers on the chemical, thermal, and mechanical properties of epoxy resin composites was studied. It was revealed that addition of ZnO NPs decreases the thermal properties of the materials because ZnO tends to form free oxygen and oxygen vacancies. The TEM images indicated that the HNT and used ZnO NPs do not tend to form any agglomerates in the structure of synthesized epoxy resin composites. Nanoindentation results shown that the epoxy resin composite with HNT and ZnO-ODTES present a good elastic behavior and surface hardness (~187.6 MPa) compared to the other samples. The epoxy resin composite without ZnO NPs has a smooth surface and the presence of the scratch does not lead to an increase in surface roughness (~40 nm). The hardness for this sample decrease with reference to the samples that contain HNT and ZnO NPs and this is due to the low of porosity and because of more micro cavities. Increasing the elastic component in the structured material indirectly contributes to the reliability of the coating and its impact behavior. Among the synthesized epoxy composites, sample containing HNT-ZnO-ODTES nanofillers has optimal properties for the final applications of the composite, especially in the naval field where the surface is regularly exposed to forces of friction and impact with seawater.

Author Contributions: Conceptualization, R.Ş. and F.O.; methodology, S.M., D.M.S.V. and C.M.S.; formal analysis, R.Ş., A.R.G., B.T., G.-M.T. and C.-A.N.; investigation, D.M.S.V., G.-M.T. and C.M.S.; data curation, S.M., A.R.G., Z.V. and C.-A.N.; writing—original draft preparation, R.Ş., Z.V. and F.O.; writing—review and editing, R.Ş., Z.V., C.-A.N., G.-M.T. and B.T. All authors have read and agreed to the published version of the manuscript.

Institutional Review Board Statement: Not applicable.

Informed Consent Statement: Not applicable.

Data Availability Statement: The data are not publicly available due to their containing information that could compromise the privacy of research participants.

Conflicts of Interest: The authors declare no conflict of interest.

References

1. Alam, M.A.; Samad, U.A.; Anis, A.; Alam, M.; Ubaidullah, M.; Al-Zahrani, S.M. Effects of SiO_2 and zno nanoparticles on epoxy coatings and its performance investigation using thermal and nanoindentation technique. *Polymers* **2021**, *13*, 1490. [CrossRef] [PubMed]
2. Samad, U.A.; Alam, M.A.; Anis, A.; Sherif, E.-S.M.; Al-Mayman, S.I.; Al-Zahrani, S.M. Effect of incorporated ZnO nanoparticles on the corrosion performance of SiO_2 nanoparticle-based mechanically robust epoxy coatings. *Materials* **2020**, *13*, 3767. [CrossRef] [PubMed]
3. Abdellaoui, H.; Raji, M.; Bouhfid, R.; Qaiss, A.e.k. Investigation of the deformation behavior of epoxy-based composite materials. In *Failure Analysis in Biocomposites, Fibre-Reinforced Composites and Hybrid Composites*, 2nd ed.; Jawaid, M., Thariq, M., Saba, N., Eds.; Elsevier: Amsterdam, The Netherlands, 2019; pp. 29–49.
4. Junid, R.; Siregar, J.P.; Endot, N.A.; Razak, J.A.; Wilkinson, A.N. Optimization of Glass Transition Temperature and Pot Life of Epoxy Blends Using Response Surface Methodology (RSM). *Polymers* **2021**, *13*, 3304. [CrossRef] [PubMed]
5. Liu, X.; Chen, X.; Ren, J.; Chang, M.; He, B.; Zhang, C. Effects of nano-ZnO and nano-SiO_2 particles on properties of PVA/xylan composite films. *Int. J. Biol. Macromol.* **2019**, *132*, 978–986. [CrossRef] [PubMed]
6. Becker, O.; Varley, R.; Simon, G. Morphology, thermal relaxations and mechanical properties of layered silicate nanocomposites based upon high-functionality epoxy resins. *Polymer* **2002**, *43*, 4365. [CrossRef]
7. Rashvand, M.; Ranjbar, Z.; Rastegar, S. Preserving Anti-Corrosion Properties of Epoxy Based Coatings Simultaneously Exposed to Humidity and UV-Radiation Using Nano Zinc Oxide. *J. Electrochem. Soc.* **2012**, *159*, C129. [CrossRef]
8. Sunny, A.T.; Vijayan, P.P.; Adhikari, R.; Mathew, S.; Thomas, S. Copper oxide nanoparticle in an epoxy network: Microstructure, chain confinement and mechanical behavior. *Phys. Chem. Chem. Phys.* **2016**, *18*, 19655–19667. [CrossRef] [PubMed]
9. Suntako, R. Cure Characteristics and Mechanical Properties of ZnO Nanoparticles as Activator in Unfilled Natural Rubbe. *Adv. Mater. Res.* **2014**, *1044–1045*, 23–26. [CrossRef]
10. Ding, K.H.; Wang, G.L.; Zhang, M. Characterization of mechanical properties of epoxy resin reinforced with submicron-sized ZnO prepared via in situ synthesis method. *Mater. Des.* **2011**, *32*, 3986–3991. [CrossRef]
11. Thipperudrappa, S.; Ullal Kini, A.; Hiremath, A. Influence of zinc oxide nanoparticles on the mechanical and thermal responses of glass fiber-reinforced epoxy nanocomposites. *Polym. Compos.* **2020**, *41*, 174e81. [CrossRef]
12. Liu, C.; Daneshvar, F.; Hawkins, S.; Kotaki, M.; Sue, H.J. High dielectric constant epoxy nano-composites containing ZnO quantum dots decorated carbon nanotube. *J. Appl. Polym. Sci.* **2020**, *138*, e49778. [CrossRef]
13. Samad, U.A.; Alam, M.A.; Chafidz, A.; Al-Zahrani, S.M.; Alharthi, N.H. Enhancing mechanical properties of epoxy/polyaniline coating with addition of ZnO nanoparticles: Nanoindentation characterization. *Prog. Org. Coat.* **2018**, *119*, 109–115. [CrossRef]
14. Srikanth, C.; Madhu, G.M. Effect of nano CdO-ZnO content on structural, thermal, optical, mechanical and electrical properties of epoxy composites. *J. Met. Mater. Miner.* **2023**, *33*, 38–52. [CrossRef]
15. Hardoň, Š.; Kúdelčík, J.; Trnka, P.; Totzauer, P.; Hornak, J.; Michal, O. The influence of ZnO nanoparticles on the dielectric properties of epoxy resin. In Proceedings of the Applied Physics of Condensed Matter, Strba, Slovakia, 19–21 June 2019.
16. Al-Lhaibi, S.A.; Al-Shabander, B.M. Study the effect of ZnO nanoparticles reinforced sawdust /epoxy composites on mechanical properties. *Dig. J. Nanomater. Biostruct.* **2022**, *17*, 851–860. [CrossRef]
17. Lorero, I.; Campo, M.; Del Rosario, G.; López, F.A.; Prolongo, S.G. New Manufacturing Process of Composites Reinforced with ZnO Nanoparticles Recycled from Alkaline Batteries. *Polymers* **2020**, *12*, 1619. [CrossRef] [PubMed]
18. Guo, L.; Zhang, Z.; Kang, R.; Chen, Y.; Hou, X.; Wu, Y.; Wang, M.; Wang, B.; Cui, J.; Jiang, N.; et al. Enhanced thermal conductivity of epoxy composites filled with tetrapod-shaped ZnO. *RSC Adv.* **2018**, *8*, 12337–12343. [CrossRef]
19. Hawkins, S.A.; Yao, H.; Wang, H.; Sue, H.J. Tensile properties and electrical conductivity of epoxy composite thin films containing zinc oxide quantum dots and multi-walled carbon nanotubes. *Carbon* **2017**, *115*, 18–27. [CrossRef]
20. Halder, S.; Prasad, T.; Khan, N.I.; Goyat, M.S.; Chauhan, S.R. Superior mechanical properties of poly vinyl alcohol-assisted ZnO nanoparticle reinforced epoxy composites. *Mater. Chem. Phys.* **2017**, *192*, 198–209. [CrossRef]
21. Sari, M.G.; Vahabi, H.; Gabrion, X.; Laheurte, P.; Zarrintaj, P.; Formela, K.; Saeb, M.R. An attempt to mechanistically explain the viscoelastic behavior of transparent epoxy/starch-modified ZnO nanocomposite coatings. *Prog. Org. Coat.* **2018**, *119*, 171–182. [CrossRef]
22. Shi, X.; Nguyen, T.A.; Suo, Z.; Liu, Y.; Avci, R. Effect of nanoparticles on the anticorrosion and mechanical properties of epoxy coating. *Surf. Coat. Technol.* **2009**, *204*, 237–245. [CrossRef]
23. Tonelli, M.; Perini, I.; Ridi, F.; Baglioni, P. Improving the properties of antifouling hybrid composites: The use of Halloysites as nano-containers in epoxy coatings. *Colloids Surf. A Physicochem. Eng. Asp.* **2021**, *623*, 126779. [CrossRef]
24. Kaybal, H.B.; Ulus, H.; Avcı, A. Seawater aged basalt/epoxy composites: Improved bearing performance with halloysite nanotube reinforcement. *Fibers Polym.* **2021**, *22*, 1643–1652. [CrossRef]

25. Pourhashem, S.; Saba, F.; Duan, J.; Rashidie, A.; Guan, F.; Nezhad, E.G.; Hou, B. Polymer/Inorganic nanocomposite coatings with superior corrosion protection perfor-mance: A review. *J. Ind. Eng. Chem.* **2020**, *88*, 29–57. [CrossRef]

26. Purcar, V.; Şomoghi, R.; Niţu, S.G.; Nicolae, C.-A.; Alexandrescu, E.; Gîfu, I.C.; Gabor, A.R.; Stroescu, H.; Ianchiş, R.; Căprărescu, S.; et al. The Effect of Different Coupling Agents on Nano-ZnO Materials Obtained via the Sol–Gel Process. *Nanomaterials* **2017**, *7*, 439. [CrossRef] [PubMed]

27. Somoghi, R.; Purcar, V.; Alexandrescu, E.; Gifu, I.C.; Ninciuleanu, C.M.; Cotrut, C.M.; Oancea, F.; Stroescu, H. Synthesis of Zinc Oxide Nanomaterials via Sol-Gel Process with Anti-Corrosive Effect for Cu, Al and Zn Metallic Substrates. *Coatings* **2021**, *11*, 444. [CrossRef]

28. *ASTM D 3363*; Standard Test Method for Film Hardness by Pencil Test. ASTM International: West Conshohocken, PA, USA, 2022.

29. Vuluga, Z.; Corobea, M.; Elizetxea, C.; Ordonez, M.; Ghiurea, M.; Raditoiu, V.; Nicolae, C.; Florea, D.; Iorga, M.; Somoghi, R.; et al. Morphological and Tribological Properties of PMMA/Halloysite Nanocomposites. *Polymers* **2018**, *10*, 816. [CrossRef] [PubMed]

30. Arat, R.; Uyanık, N. Surface Modification of Nanoclays with Styrene-Maleic Anhydride Copolymers. *Nat. Resour.* **2017**, *8*, 159–171. [CrossRef]

31. Thakura, S.; Bhattacharyab, R.; Neogia, S.; Neogi, S. Enhancement of Microwave Absorption Properties of Epoxy by Sol–Gel-Synthesised ZnO Nanoparticles. *Indian Chem. Eng.* **2016**, *58*, 310–324. [CrossRef]

32. Dhanapal, D.; Ranjitha, J.; Vijayalakshmi, S.; Sagadevan, S. Fabrication of tetraglycidyl epoxy nano-composites functionalized with amine-terminated zinc oxide with improved mechanical and thermal properties. *J. Mater. Res. Technol.* **2022**, *21*, 3947–3960. [CrossRef]

33. Ramírez-Herrera, C.A.; Cruz-Cruz, I.; Jiménez-Cedeño, I.H.; Martínez-Romero, O.; Elías-Zúñiga, A. Influence of the Epoxy Resin Process Parameters on the Mechanical Properties of Produced Bidirectional [±45°] Carbon/Epoxy Woven Composites. *Polymers* **2021**, *13*, 1273. [CrossRef] [PubMed]

34. Moussa, S.; Namouchi, F.; Guermazi, H. Elaboration, structural and optical investigations of ZnO/epoxy nanocomposites. *Eur. Phys. J. Plus* **2015**, *130*, 152. [CrossRef]

35. Thakor, S.G.; Rana, V.A.; Vankar, H.P.; Pandit, T.R. Dielectric spectroscopy and structural characterization of nano-filler-loaded epoxy resin. *J. Adv. Dielectr.* **2021**, *11*, 2150011. [CrossRef]

36. Ramezanzadeh, B.; Attar, M.M.; Farzam, M. Effect of ZnO nanoparticles on the thermal and mechanical properties of epoxy-based nanocomposite. *J. Therm. Anal. Calorim.* **2011**, *103*, 731–739. [CrossRef]

37. Vuluga, Z.; Sanporean, C.-G.; Panaitescu, D.M.; Teodorescu, G.M.; Corobea, M.C.; Nicolae, C.A.; Gabor, A.R.; Raditoiu, V. The Effect of SEBS/Halloysite Masterbatch Obtained in Different Extrusion Conditions on the Properties of Hybrid Polypropylene/Glass Fiber Composites for Auto Parts. *Polymers* **2021**, *13*, 3560. [CrossRef] [PubMed]

38. Tran, T.N.; Pham, T.V.A.; Le, M.L.P.; Nguyen, T.P.T.; Tran, V.M. Synthesis of amorphous silica and sulfonic acid functionalized silica used as reinforced phase for polymer electrolyte membrane. *Adv. Nat. Sci. Nanosci.* **2013**, *4*, 045007. [CrossRef]

39. Ravindra, R.T.; Kaneko, S.; Endo, T.; Lakshmi, R.S. Spectroscopic Characterization of Bentonite. *J. Laser Opt. Photonics* **2017**, *4*, 171.

40. Wu, Z.; Li, S.; Liu, M.; Wang, Z.; Liu, X. Liquid oxygen compatible epoxy resin: Modification and characterization. *RSC Adv.* **2015**, *5*, 11325–11333. [CrossRef]

41. Du, M.; Guo, B.; Lei, Y.; Liu, M.; Jia, D. Carboxylated butadiene–styrene rubber/halloysite nanotube nanocomposites: Interfacial interaction and performance. *Polymer* **2008**, *49*, 4871–4876. [CrossRef]

42. Lim, K.; Chow, W.S.; Pung, S.Y. Accelerated Weathering and UV Protection-Ability of Poly(Lactic Acid) Nanocomposites Containing Zinc Oxide Treated Halloysite Nanotube. *J. Polym. Environ.* **2019**, *27*, 1746–1759. [CrossRef]

43. Muhammad, A.N.S.; Farooq, A.; Lodhi, M.; Deen, K. Performance evaluation of epoxy coatings containing different fillers in natural and simulated environmental conditions for corrosion resistance. *J. Biomed. Eng. Biosci.* **2019**, *3*, 1.

44. Tomaszewska, J.; Sterzyński, T.; Woźniak-Braszak, A.; Banaszak, M. Review of Recent Developments of Glass Transition in PVC Nanocomposites. *Polymers* **2021**, *13*, 4336. [CrossRef] [PubMed]

45. Hsu, S.C.; Whang, W.T.; Hung, C.H.; Chiang, P.C.; Hsiao, K.N. Effect of the polyimide structure and ZnO concentration on the morphology and characteristics of polyimide/ZnO nanohybrid films. *Macromol. Chem. Phys.* **2005**, *206*, 291–298. [CrossRef]

46. Baghdadi, Y.N.; Youssef, L.; Bouhadir, K.; Harb, M.; Mustapha, S.; Patra, D.; Tehrani-Bagha, A.R. The effects of modified zinc oxide nanoparticles on the mechanical/thermal properties of epoxy resin. *J. Appl. Polym. Sci.* **2020**, *137*, 49330. [CrossRef]

47. Ammar, S.; Ramesh, K.; Vengadaesvaran, B.; Ramesh, S.; Arof, A.K. Amelioration of anticorrosion and hydrophobic properties of epoxy/PDMS composite coatings containing nano ZnO particles. *Prog. Org. Coat.* **2016**, *92*, 54–65. [CrossRef]

48. Adroja, P.P.; Ghumara, R.Y.; Parsania, P.H. Dynamic DSC curing kinetic study of epoxy resin of 1,3-bis(4-hydroxyphenyl) prop-2-en-1-one using aromatic diamines and phthalic anhydride. *J. Appl. Polym. Sci.* **2013**, *130*, 572–578. [CrossRef]

49. Lizundia, E.; Serna, I.; Axpe, E.; Vilas, J.L. Free-volume effects on the thermomechanical performance of epoxy-SiO$_2$ nanocomposites. *J. Appl. Polym. Sci.* **2017**, *134*, 45216. [CrossRef]

50. Panahandeh, N.; Torabzadeh, H.; Aghaee, M.; Hasani, E.; Safa, S. Effect of incorporation of zinc oxide nanoparticles on mechanical properties of conventional glass ionomer cements. *J. Conserv. Dent. Endod.* **2018**, *21*, 130–135.

51. Li, J.H.; Hong, R.Y.; Li, M.Y.; Li, H.Z.; Zheng, Y.; Ding, J. Effects of ZnO nanoparticles on the mechanical and antibacterial properties of polyurethane coatings. *Prog. Org. Coat.* **2009**, *64*, 504–509. [CrossRef]

52. Karasinski, E.N.; Da Luz, M.G.; Lepienski, C.M.; Coelho, L.A.F. Nanostructured coating based on epoxy/metal oxides: Kinetic curing and mechanical properties. *Thermochim. Acta* **2013**, *569*, 167–176. [CrossRef]

53.	Vlad-Cristea, M.; Riedl, B.; Blanchet, P.; Jimenez-Pique, E. Nanocharacterization techniques for investigating the durability of wood coatings. *Eur. Polym. J.* **2012**, *48*, 441–453. [CrossRef]
54.	Skaja, A.; Fernando, D.; Croll, S. Mechanical property changes and degradation during accelerated weathering of polyesterurethane coatings. *J. Coat. Technol. Res.* **2006**, *3*, 41–51. [CrossRef]
55.	Parimalam, M.; Islam, M.R.; Yunus, R.M. Effects of nanosilica, zinc oxide, titatinum oxide on the performance of epoxy hybrid nanocoating in presence of rubber latex. *Polym. Test.* **2018**, *70*, 197–207. [CrossRef]